



## Differences between 3-D printed and traditionally milled CoCr dental alloy from casted block in oral environment

Mirjam Bajt Leban<sup>a,\*</sup>, Matej Kurnik<sup>b</sup>, Igor Kopač<sup>b</sup>, Matic Jovičević Klug<sup>c</sup>, Bojan Podgornik<sup>c</sup>, Tadeja Kosec<sup>a</sup>

<sup>a</sup> Slovenian National Building and Civil Engineering Institute, Dimičeva ulica 12, Ljubljana, Slovenia

<sup>b</sup> Medical Faculty, University of Ljubljana, Vrazov trg 22, Ljubljana, Slovenia

<sup>c</sup> Institute of Metals and Technology, Lepi pot 11, 1000 Ljubljana, Slovenia

### ARTICLE INFO

#### Keywords:

CoCr dental alloy  
Selective laser melting  
Corrosion  
Ion release  
Artificial saliva

### ABSTRACT

The aim of this study was to compare corrosion resistance and ion release in CoCr dental alloys with identical chemical compositions produced using different technologies (SLM – selective laser melting and milling from cast blocks) and heat treatment (SLM parts only). The corrosion properties were tested in artificial saliva, artificial saliva with fluoride ions, and artificial saliva with added lactic acid to simulate inflammations. The study included electrochemical tests, microstructural investigation and ion release tests in the three different environments for a total of 42 days. The best performance of CoCr as a result of potentiodynamic polarization was observed in the artificial saliva with added lactic acid, which is in contradiction with the highest ion release measured from all the materials tested and electrochemical impedance spectroscopy that showed a deterioration of the passive layer in an acidic environment. Microstructural investigation revealed that different phases precipitated by heat treatment trigger increased release of Mo and W ions. The printing method does not raise critically ion release from CoCr alloy, while the state of the surface greatly impacts the extent of the ion release. This study demonstrates the importance of an interdisciplinary approach to the study of corrosion and biocompatibility in dental alloys.

### 1. Introduction

Despite the fact that many high strength ceramic systems, such as stabilized zirconia, alumina and lithium disilicate ceramics [1], are available in clinical dentistry, metal alloys still play an important role as the material of choice for prosthodontic treatment in everyday clinical practice. Due to their favourable characteristics and acceptable price, metal alloys such as CoCr alloys play nowadays a predominant role amongst metals used in dentistry. In fixed prosthodontics CoCr alloys are used for metal frameworks in porcelain-metal-fused crowns and bridges, in removable prosthodontics they are used for metal frameworks in partial dentures, and in implant prosthodontic treatment they are used for metal suprastructures. Additionally, with the introduction of CAD-CAM technologies (computer aided design–computer aided manufacturing) and different subtractive and additive production modalities, the use of these alloys has risen in popularity with dentists and dental laboratories [2].

Additive manufacturing (AM) technologies have the advantages of

saving material and reducing production time, yet it is precise and costly compared to milling and casting procedures [3]. One commonly-used AM processing technique is selective laser melting (SLM). The mechanical properties of metal frameworks produced from CoCr alloys using SLM are superior to those cast or milled, exhibiting higher surface hardness, yield strength and tensile strength [4,5]. The surfaces of objects produced using SLM are rough and in most cases should be additionally machined on the outer surface. The rough as-built surface can reduce the mechanical, fatigue and corrosion properties of an object [6–8]. Before use in clinical practice the surface is usually sandblasted with aluminium oxide particles [9,10]. The purpose of this procedure is to remove any surface impurities and metal oxides and to flatten the rough surface which occurs as a consequence of the printing technology.

In addition to having good mechanical properties, dental alloys used intraorally also need to be corrosion resistant and biocompatible, and should not contain any diffusible metallic elements that could be deposited into the surrounding oral tissues. Metal ions released from alloys can cause an inflammatory tissue response, allergic reactions, cell

\* Corresponding author.

E-mail address: [mirjam.leban@zag.si](mailto:mirjam.leban@zag.si) (M.B. Leban).

<https://doi.org/10.1016/j.electacta.2023.142066>

Received 28 July 2022; Received in revised form 4 January 2023; Accepted 16 February 2023

Available online 19 February 2023

0013-4686/© 2023 The Author(s). Published by Elsevier Ltd. This is an open access article under the CC BY-NC-ND license (<http://creativecommons.org/licenses/by-nc-nd/4.0/>).

necrosis and unaesthetic staining on the gingival margin or the teeth [11,12]. Saliva and other external factors create an extremely aggressive biomechanical environment in the oral cavity, so the corrosion resistance and chemical stability of dental alloys is essential for clinical success [13].

The excellent corrosion resistance and biocompatibility of CoCr alloys is based on the instantaneous development of an oxide layer on the metal surface in the presence of air. A passive layer of Cr-oxide (usually  $\text{Cr}_2\text{O}_3$ ), a few nm thick, prevents a fast reaction of the dental alloy and the transition of metallic elements into the surrounding oral tissues [12]. The main elements of CoCr alloys, Co and Cr, are toxic, "per-se", even at low concentrations. According to European Chemicals Agency (ECHA) the following properties of concern of Co (CAS no.: 7440-48-4) are listed: suspected to be mutagenic, toxic to reproduction and skin and respiratory sensitising. The rate of release into tissue is therefore very important [14]. It has been found in several studies [15,14] that the release of Co into synthetic saliva is lower in objects produced by SLM compared to those manufactured conventionally [16]. Additionally, the longer the exposure time, the greater the difference in total metal ion release is between objects produced by SLM and conventionally. The acidity of saliva significantly influences the release of Co ions [15,17]. CoCr alloys are additionally alloyed with Mo and W. Mo increases resistance to pitting corrosion by enabling the creation of a passive film, while W enhances the structural and chemical stability of the alloy and improves the effects of preoxidation [18–20].

The phenomenon of metal ion release is strongly related to the corrosion resistance of a metal alloy that interacts with saliva in an oral environment or body fluid in tissues [21]. Many studies have examined the corrosion behaviour, ion release and biocompatibility of CoCr alloys manufactured in different ways. Some researchers have compared the corrosion properties [22], while research comparing the ion release between alloys manufactured using different processes, including DED (direct energy deposition), casting and the wrought process, reported that ion release is higher in cast objects compared to other specimens [18,23]. Kassapidou and co-workers [24] studied the ion release in CoCr alloys manufactured using four different techniques. They concluded that the cast and milled specimens exhibited the highest ion release in acidic conditions [25]. The lowest ion release detected occurred when the alloy was fabricated from virgin powder by 3-D printing [26].

The composition of alloying elements [19], and the heat treatment applied, play an important role in the behaviour of the CoCr alloys [27]. Heat treatment is, however, even more important in the case of SLM fabricated parts, which frequently exhibit a columnar-cellular dendritic structure due to the rapid cooling rates and thermal gradients that occur under local solidification conditions. This exerts a strong anisotropy on the microstructure and affects the ductility, mechanical properties and residual stresses [28]. In »in vitro« testing of the biocompatibility of CoCr alloys fabricated using the SLM method, it was observed that the rapid rate of cooling and fine cellular microstructure led to the material having a higher corrosion resistance than a cast CoCr alloy [29]. Xin and co-workers [3] also found a more homogeneous microstructure and thus higher corrosion resistance in specimens fabricated using the SLM method compared to cast samples.

Cast CoCr alloys mainly exhibit a mixture of  $\gamma$  (face-centred cubic - FCC) and  $\epsilon$  (hexagonal close-packed - HCP) phases. Although the brittle  $\epsilon$  phase in as-build SLM parts starts to fade away, the ductile  $\gamma$  phase, accompanied by low-intensity peaks of the  $\sigma$  phase, are only obtained after solution heat treatment [30,31]. It has also been observed in many heat treatment experiments that  $\text{M}_{23}\text{C}_6$  type carbides precipitate along the grain boundaries [27]. Heat treatment also eliminates crystal defects, such as dislocations, and stabilizes the microstructure which leads to the reduction of residual stress [17,32]. In this respect, the temperature of the solution heat treatment is the most important factor, affecting the strength, ductility and hardness of the alloy and thus influencing its fracture strength, fatigue life and wear resistance. It may also affect the corrosion resistance, as indicated by some authors [27,

33]. The influence of different heat treatment temperatures and times has been extensively investigated in the past [27,29,33–38]. The best results were observed at a temperature 1050 °C, with the properties deteriorating at lower temperatures due to a sensitive  $\gamma \rightarrow \epsilon$  transformation region, and at higher temperatures due to grain growth [34]. Treatment time, on the other hand, has a lesser effect [39].

The aim of the present study was to investigate the corrosion properties of CoCr specimens manufactured using different technologies, namely by SLM, additionally heat treated SLM and from cast alloy for milling with identical chemical compositions. Corrosion properties were evaluated by short and long-term electrochemical tests and 42-day ion migration in artificial saliva, artificial saliva containing fluoride and acidified artificial saliva at 37 °C. The results of the electrochemical testing and ion release measurements were supported by detailed metallographic and surface roughness characterization.

The hypotheses were that different manufacturing processes and thermal treatments lead to different levels of corrosion resistance, and that the results of the electrochemical tests lead to the same conclusion as the results of the ion migration tests.

## 2. Materials and methods

Three different CoCr alloy specimens were examined, each having the same chemical composition, containing 59% Co, 27% Cr, 9.5% W, 3.5% Mo, 1% Si and less than 1% of C, Fe, Mn and N, as provided by S&S Scheftner GmbH, Dental alloys. The first specimen was 3D-printed using the selective laser method (denoted as SLM), while the second was then additionally heat treated at 1050 °C and furnace cooled (denoted as SLM-HT). Laser power was set at 70 W, laser travel velocity of 520 mm/s, hatch distance of 25  $\mu\text{m}$  and a layer thickness of 25  $\mu\text{m}$ . The calculated energy density was 215.4 J/mm<sup>3</sup>. The dimensions of the SLM and SLM-HT specimens fabricated for the electrochemical tests were 8 × 8 × 8 mm<sup>3</sup>, with the exposed surface area being 0.64 cm<sup>2</sup>. For the ion migration tests the SLM printed specimens were cylindrical in shape, with a diameter of 10 mm, a length of 30 mm, and a total exposed area of 11.0 cm<sup>2</sup> for each specimen. The third specimen was milled from a casted prefabricated block (denoted as REF). REF specimens for electrochemical measurement were cylindrical in shape with a 6 mm diameter, with total exposed area of 0.28 mm<sup>2</sup>. REF specimens for the ion migration tests were also cylindrical, with a diameter of 6 mm and length of 50 mm, giving a total exposed area of 10 cm<sup>2</sup>.

Metallographical investigation was performed on the cross-section transverse to the building direction in the SLM specimens, and transverse to the axis of the shorter milling disc in the case of the reference specimens. All specimens were ground and polished until a mirrored surface was achieved, and then electrolytically etched in 100 ml  $\text{H}_2\text{O}$  + 4 ml HCl, by applying a voltage of 5 V for 6 s, in order to reveal the microstructure. Microstructural examination was performed by light microscopy (Zeiss Axio Imager.Z2m with Zen software, Carl Zeiss AG, Germany, 2008), using bright-field and polarized light. Samples were also investigated via scanning electron microscopy (SEM) (Jeol JSM-6500F, Jeol Ltd., Japan, 2019) using secondary electron imaging (SEI) and backscattered electron imaging (BSE). The chemical composition of individual areas was probed using energy-dispersive X-ray spectroscopy (EDS) with a 15 keV electron beam (Oxford EDS INCA Energy 450, detector type INCA X-SIGHT LN2, Oxford Instruments, UK).

Electrochemical tests were performed using a Gamry 600 Ref+ potentiostat in a sequence containing non-destructive measurements: open circuit potential measurement (OCP) for 6200 s, and linear polarization (LP) in a range  $\pm 20$  mV (vs  $E_{\text{corr}}$ ) at a scan rate 0.1 mV/s. Electrochemical sequencing was finished with destructive potentiodynamic polarization (PD), starting at  $-250$  mV cathodically vs  $E_{\text{corr}}$  then increasing in the anodic direction up to 1.2 V at a scan rate of 1 mV/s. Three-electrode corrosion cell was used, with the working electrode embedded in a Teflon holder. An Ag/AgCl electrode served as the reference electrode and glassy carbon used for the counter electrode.

Unless otherwise stated, all potentials are presented with respect to the silver/ silver chloride electrode (Ag/AgCl).

For the long-term electrochemical impedance spectroscopy measurements, the frequency ranged from 65 kHz to 1 mHz, at 7 points per decade and an AC amplitude of  $\pm 10$  mV. The absolute impedance and phase angle were measured at each frequency. The impedance measurements were carried out at open circuit potential (OCP) after various times of immersion (1 h, 4 h, 8 h, 24 h, 48 h, 72 h, 96 h, 120 h, 144 h and 168 h) in the artificial saliva at 37 °C. The impedance data were interpreted on the basis of equivalent electrical circuits, using the Zview (Scribner) program for fitting the experimental data. The chi square values for goodness of fit were between 0.0001 and 0.005. Before all electrochemical tests all specimens were ground with SiC grinding paper up to 1200 grit, rinsed by deionized water and ethanol, and dried at the air.

The ion migration tests were performed according to the standard ISO 10,271: 2020 (Dentistry — Corrosion test methods for metallic materials). Before exposure all specimens were sandblasted with 110  $\mu\text{m}$  particles of aluminium oxide, then cleaned with ethanol in an ultrasound bath for 15 min and air-dried. 1 ml of test solution per  $\text{cm}^2$  of the exposed specimen area was poured into each cuvette for a given period, then, according to the prescribed schedule, the testing solution was exchanged for the new one, and the previous solution tested. The ion migration test lasted 42 days in total. The solution for the ion release test was extracted after days 1, 4, 7, 14, 21, 28, 35 and 42, and replaced each time with a freshly prepared solution. In order to assure repeatability, three specimens of each type of specimen were exposed to each type of

solution. The amount of Co, Cr, W and Mo ions in the solutions sampled were measured using an ICP-MS Agilent 7900x, Agilent Technologies, Japan (2019).

Both the electrochemical and the ion migration tests were performed at a constant temperature of 37 °C. The solution for both tests was artificial saliva (AS) with a chemical composition as follows: 0.6 g/L NaCl, 0.72 g/L KCl, 0.22 g/L  $\text{CaCl}_2 \cdot 2 \text{H}_2\text{O}$ , 0.68 g/L  $\text{KH}_2\text{PO}_4$ , 0.856 g/L  $\text{Na}_2\text{HPO}_4 \cdot 12 \text{H}_2\text{O}$ , 0.060 g/L KSCN, 1.5 g/L  $\text{KHCO}_3$  and 0.03 g/L citric acid [40]. The pH of this solution was  $6.5 \pm 0.1$ . The electrochemical tests were also conducted in saliva containing 1450  $\mu\text{g}/\text{mL}$  of fluoride ions, through the addition of 3.15 g/L NaF (AS + NaF), and acidified saliva (AS + lactic acid), containing 0.1 mol/L of lactic acid, with a pH of  $2.3 \pm 0.1$ . Ion migration tests in artificial saliva with added F<sup>-</sup> ions and the acidic artificial saliva solution were only carried out on the SLM specimens (including those heat treated).

The ion release test results were analysed using IBM® SPSS statistical software (version 22). Data were presented as means and standard deviations (SD). A *t*-test was used to investigate the difference between the two groups, while a two-way ANOVA was applied for comparison of more than two groups. A *p*-value lower than 0.05 was deemed to be significant.

Since the surface appearance of the milled and 3D printed specimens differed significantly, despite the fact that the surface sandblasting protocol before the migration test was identical, the actual area of both types of specimen was compared using a ZEISS LMS 700 confocal laser microscope, using a 405 nm laser at 200  $\times$  magnification.

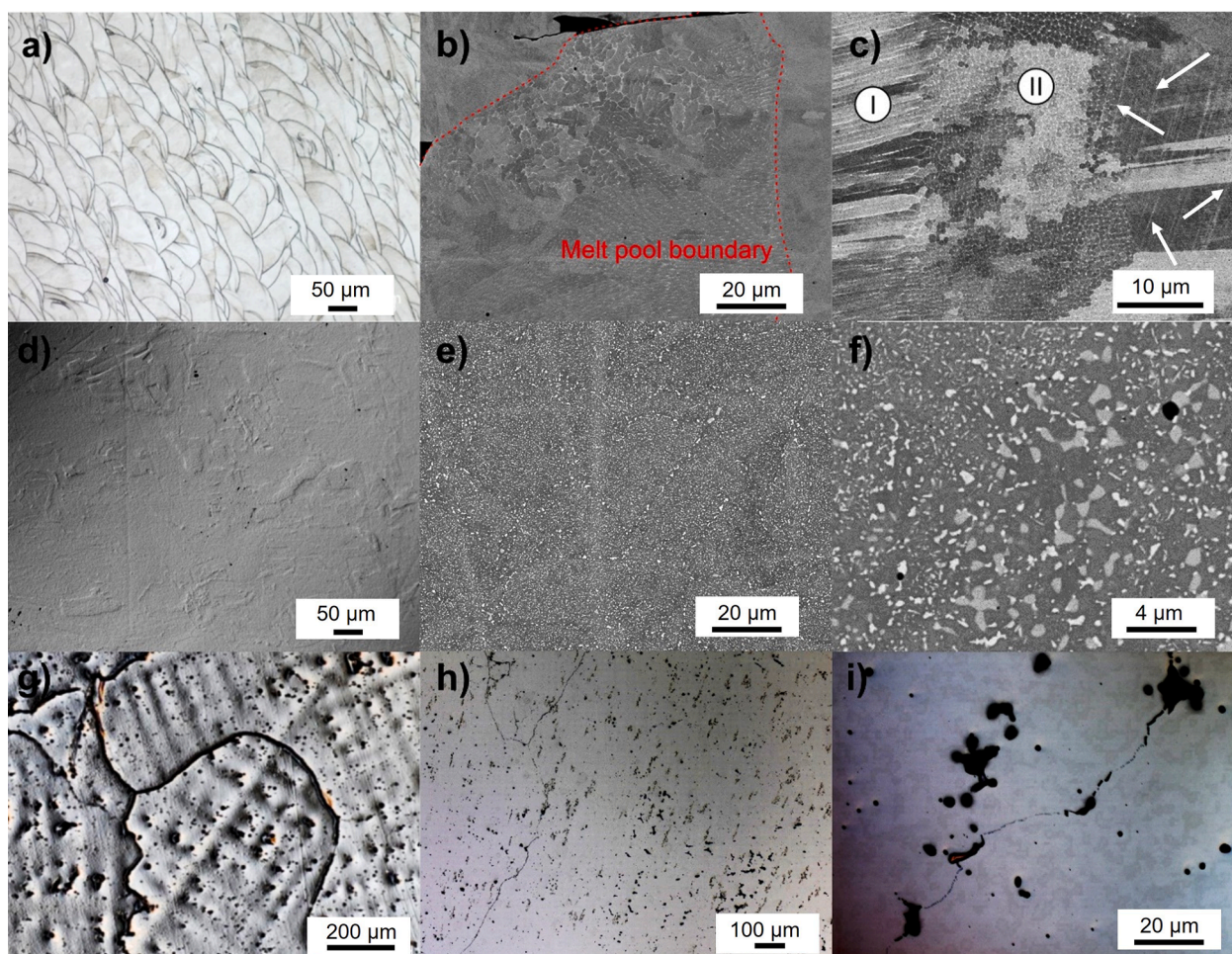


**Fig. 1.** Microstructural images of the CoCr specimens produced by different methods and with or without heat treatment: a) to c) the SLM specimen, d) to f) the SLM specimen heat treated at 1050 °C and g) to i) the reference specimen.

### 3. Results

#### 3.1. Microstructural properties

The micrographs of the various samples presented in Fig. 1 clearly indicate the different microstructures developed due to the manufacturing process used and the application of heat treatment during production.

Following production the SLM samples display a characteristic formation of overlapping regions of melting pools (Fig. 1a) that are defined in shape and texture based on the parameters of the SLM printing [14, 41]. The dominating  $\gamma$  (fcc) phase is present with a small quantity of the  $\epsilon$  (hcp) martensitic phase, which can be seen as bands in the accompanying SEM image (marked with white arrows in Fig. 1c). The columnar structure is presented in Fig. 1b (due to the cellular-like form of the cross-sectioning, it is also denoted as a cellular structure), which defines the regional orientation of sub-micron crystallites in groups that preferentially grow with their long axis along the highest thermal gradient. The columnar structures can be observed inside the melting pools (Fig. 1b). The orientation of smaller groupings can, however, deviate within a given melt pool (see the regions marked I and II in Fig. 1c).

The heat-treated SLM produced specimen (SLM-HT), the microstructure of which can be seen in Fig. 1d-f, displays less pronounced features associated with the previous (SLM) grown structures (Fig. 1d). The reduced texture effect occurs due to the precipitation of additional phases and redistribution of the alloying elements. As such, the original melt pool structures and the columnar structure dissolve and reform, leaving behind an arrangement pattern of various precipitates (Fig. 1e). The selective growth of individual phases occurs due to the differing chemical concentrations within individual regions of the prior microstructure. Fine needle-like precipitation, enriched with Cr (approximately 30 at%), develop across the material, evenly forming within the  $\gamma$  (fcc) phase. The previous melt pool boundaries are replaced by  $\text{Co}_3\text{Cr}(\text{Mo,W})_2\text{Si}$  precipitates and the  $\sigma$  phase, as was determined by additional EDS analysis. These two phases also preferentially formed when the prior microstructure had displayed enlarged columnar structures (Fig. 1f), which formed due to the overlap of the laser paths during the SLM process, causing the material to remelt locally.

Microstructural examination of the milling block samples (REF) revealed they have a dendritic microstructure (Fig. 1g). The microstructure primarily consists of the  $\gamma$  (fcc) phase, with different interdendritic regions enriched with alloying elements Mo, Co and W, as can be seen by the uneven etching effect on the microstructure (Fig. 1h). The dendritic structures also indicate a different arrangement of defects, most of which were determined to be silicon-enriched particles formed during the casting process.

#### 3.2. Electrochemical measurements

##### 3.2.1. Potentiodynamic measurements

Potentiodynamic curves for the REF, SLM and SLM-HT specimens

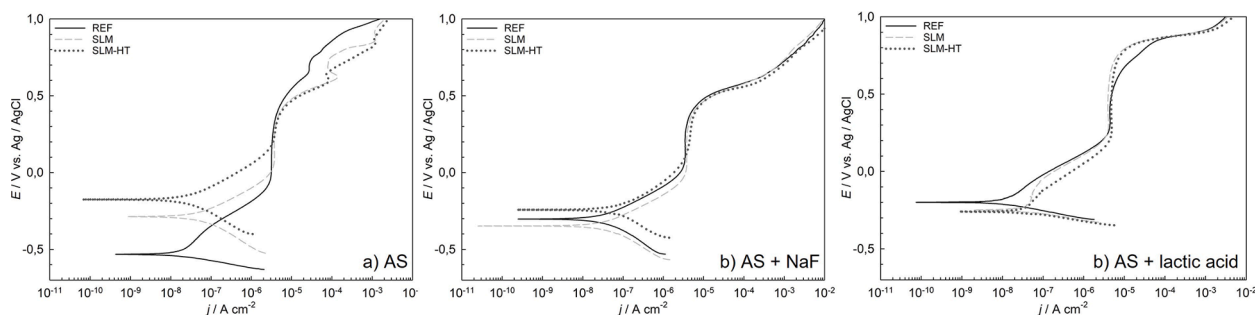


Fig. 2. Potentiodynamic polarisation curves for measurements in a) artificial saliva, b) artificial saliva with added fluoride ions and c) in artificial saliva with added lactic acid at 37 °C for the reference, SLM and heat-treated SLM specimens.

exposed in AS, AS + NaF and AS + lactic acid at 37 °C are presented in Fig. 2, showing the cathodic and anodic behaviour of the CoCr alloys in the different environments. Electrochemical parameters deduced from the PD curves of all tested material / environment pairs are gathered in the columns on the right in Table 1. Upon immersion, the measured potential started to increase in all specimens in all three environments.  $E_{\text{OCP}}$  was lowest in the REF specimen in AS (−0.399 V), and the most positive in the REF specimen in AS + lactic acid with a pH of 2.3 ( $E_{\text{OCP}} = -0.10$  V). The most positive potentials are observed in the AS + lactic acid.

Potentiodynamic (PD) curves for the CoCr samples in AS exhibited a slight increase in anodic current density more positive than  $E_{\text{corr}}$ , then a region of constant current density ( $j$ ) is formed (Fig. 2a). At a certain potential, the current started to increase, and a typical transpassive peak is observed in all the specimens in AS. The width of the passive region is related to the position of the corrosion potential, with the passive current density at 3  $\mu\text{A}/\text{cm}^2$  being widest for the REF specimen and narrowest for the SLM-HT specimen. Furthermore,  $j_{\text{corr}}$  is lowest for the REF specimen and highest for the SLM specimen, with the  $j_{\text{corr}}$  for the SLM-HT specimen lying somewhere in between.

In artificial saliva with added fluoride ions, the shape of the potentiodynamic curve is very similar across all of the specimens (Fig. 2b), while in this media the polarization resistance values ( $R_p$ ) are highest in the SLM specimen, at 0.691  $\text{M}\Omega \text{cm}^2$ , and lowest in the SLM-HT specimen ( $R_p = 0.508 \text{M}\Omega \text{cm}^2$ ). A similar tendency is observed for the corrosion current density values,  $j_{\text{corr}}$  (Table 1).

In the case of AS + lactic acid at 37 °C, it can be observed that both the OCP potentials and the PD curves are very similar across all of the materials studied i.e. the REF, SLM and SLM-HT samples (Fig. 2c). The

Table 1

Electrochemical parameters (open circuit potential -  $E_{\text{OCP}}$ , polarization resistance -  $R_p$ , corrosion potential -  $E_{\text{corr}}$ , corrosion current density -  $j_{\text{corr}}$ , and breakdown potential -  $E_b$ ) deduced from corrosion potential measurements, potentiodynamic polarization curves and linear polarization measurements.

		$E_{\text{OCP}}$	LP	PD curves			
		$E_{\text{OCP}}/\text{V}$	$R_p/\text{M}\Omega \text{cm}^2$	$E_{\text{corr}}/\text{V}$	$j_{\text{corr}}/\mu\text{A cm}^{-2}$	$E_b/\text{V}$	$E_{\text{corr}}/\text{V}$
AS	REF	−0.399	1.19	−0.532	0.0155	0.452	0.984
	SLM	−0.314	0.472	−0.287	0.0539	0.456	0.743
	SLM-HT	−0.185	0.640	−0.176	0.0278	0.460	0.636
AS + NaF	REF	−0.312	0.543	−0.303	0.032	0.447	0.750
	SLM	−0.350	0.691	−0.348	0.0352	0.437	0.785
	SLM-HT	−0.228	0.508	−0.243	0.0836	0.461	0.704
AS + lactic acid	REF	−0.10	0.857	−0.20	0.0102	0.670	0.870
	SLM	−0.101	1.05	−0.25	0.0264	0.780	1.03
	SLM-HT	−0.122	0.419	−0.260	0.0244	0.790	1.05

corrosion current density,  $j_{\text{corr}}$ , is lowest in this environment in all cases, in comparison to the AS and AS + NaF environments. The  $R_p$  values (Table 1) are the highest of all the environments tested, being  $0.857 \text{ M}\Omega \text{ cm}^2$  for the REF CoCr alloy and  $1.01 \text{ M}\Omega \text{ cm}^2$  for the SLM specimen. The SLM-HT specimen had the lowest  $R_p$  ( $0.419 \text{ M}\Omega \text{ cm}^2$ ) in the AS + lactic acid.

From the PD curves (Fig. 2) it can also be seen that the highest breakdown potential ( $E_b$ ) is observed in the AS + lactic acid in all three specimen types (0.67 mV for the REF specimen and approximately 0.78 mV and 0.79 V for the SLM and SLM-HT specimens, respectively). Furthermore, the potential window of passivity is wider in the AS + lactic acid (see  $E_b-E_{\text{corr}}$  column in Table 1). The width of the passive region is similar for all of the specimens in the AS + NaF, at around 0.75 V. A transpassive region could be identified from the shape of the potentiodynamic curve [42] in all three of the specimens exposed to AS, indicating the oxidation of  $\text{Cr}^{3+}$  to  $\text{Cr}^{6+}$ , as described by XPS analysis in the literature [43,44]. This specific phenomenon was only observed when the specimens were exposed to AS. For all specimens the current density in the passive region is very similar in all the environments tested (AS, AS + NaF, AS + lactic acid), at around  $4 \mu\text{A}/\text{cm}^2$ .

### 3.2.2. Long-term electrochemical impedance spectroscopy

The long-term behaviour of the different CoCr specimens was measured during exposure to AS and AS + lactic acid at  $37^\circ\text{C}$  for 168 h (7 days) at 1 h, 4 h, 8 h, 24 h, 48 h, 72 h, 96 h, 120 h, 144 h and 168 h. Selected electrochemical impedance spectroscopy results for the different CoCr specimens, namely spectra for the milled (REF), SLM and SLM-HT specimens measured at 24 h, 96 h and 168 h are presented as Nyquist plots in Fig. 3.

In general, the impedance spectra in Fig. 3 consist of a high frequency intercept with the abscise axis and a main frequency semicircle. The impedance spectra were fitted with the equivalent circuits represented in Fig. 3a. The lower equivalent circuit consisted of a parallel couple of resistance and capacitance elements ( $RQ$ ) in series with  $R_s$ , which represents the electrolyte resistance. The circuit represents just one possible equivalent circuit that adequately fits the impedance spectra. Previous studies of a CoCr alloy showed that the equivalent circuit in Fig. 3 gave representative values of the parameters fitted [45, 46].

The symbol  $Q$  signifies the possibility of a non-ideal capacitance (CPE, Constant Phase Element), with  $n$  varying from 0 to 1. The impedance of the CPE is given by [47]:

$$Q = Z_{\text{CPE}}(\omega) = [C(j\omega)^n]^{-1}, \quad (1)$$

where  $\omega$  is the sine wave modulation angular frequency,  $j^2 = -1$  and  $n$  is the CPE exponent. For  $n = 1$ , the  $Q$  element reduces to a capacitor with a capacitance  $C$  ( $Z_{\text{CPE}} = C$ ,  $n = 1$ ) and, for  $n = 0$ , it reduces to a simple resistor ( $Z_{\text{CPE}} = R$ ,  $n = 0$ ).

The high frequency parameters  $R_1$  and  $Q_1$  represent the properties of the growing passive film/ solution interface reactions. In the low frequency range, the process describes the capacitance of the passive layer ( $Q_2$ ), where  $R_2$  is the resistance of the passive film. In some cases, the equivalent circuit is simplified to a  $Q_2R_2$  combination in series with the solution resistance (the upper equivalent circuit in Fig. 3a). At this point the properties of the passive film were expressed more than the other reactions during the period of observation.

The values of fitted parameters of the equivalent circuit in the two different environments following different periods of immersion are presented in the Table 1 in a supplemental file for all three specimens investigated. The parameter  $R_s$  has a value between  $0.5$  and  $29 \Omega \text{ cm}^2$  and is ascribed to the electrolyte resistance. It can be seen from Table 1 in supplemental file that the  $R_1$  values are smaller than the  $R_2$  values. The  $R_1$  values represent the resistance at the interface of the metal and the growing passive layer, while  $R_2$  represents the resistance of the passive film on the CoCr dental alloy. In the REF specimen, the  $R_1$  values show that a porous layer with a very low resistance was formed. These values are higher for the SLM specimen in AS, while this process was not observed in the SLM-HT specimen. In AS + lactic acid, the SLM specimen again showed a relatively small resistance compared to the process observed at high frequencies in artificial saliva at  $37^\circ\text{C}$ . After 3 days of exposure to AS the  $R_1$  value of the SLM specimen became higher, as the effect of porosity became less pronounced. CPE, denoted as  $Q_1$  (and  $Q_2$ ), were recalculated using the following equation [48]:

$$C_1 = [R_1^{1-n} Q_1]^{1/n}, \quad (2)$$

in order to compare the capacitance values of the CoCr alloy at different immersion times for the different specimens in the two different media i. e. AS and AS + lactic acid.

The overall polarization resistance ( $R$ ) is a sum of the partial resistances,  $R_1$  and  $R_2$ , and represents the resistance to corrosion. The results of polarization resistance are presented in Fig. 4a. In AS these are slightly higher at longer immersion times for both the REF and SLM-HT specimens. With the SLM specimen, the polarization resistance slowly decreases, with the reduction being even more pronounced when the SLM specimen was exposed to the AS. The decrease in polarization resistance indicates the weakening or dissolution of the passive film/ oxide layer.

As seen from Figs. 4b and c, the  $C_1$  and  $C_2$  values are similar for all the specimens observed in both types of media and across the different immersion times.

A decrease in  $C_2$  can be attributed to a thickening of the oxide layer. This thickening is greater at lower immersion times (Fig. 4c). In the REF and SLM specimens this thickening is more pronounced in the AS, while it is very stable for both the SLM-HT specimen in AS and the SLM specimen in AS + lactic acid.

The constant value of  $C_2$  and the decrease in  $R$  could indicate that the

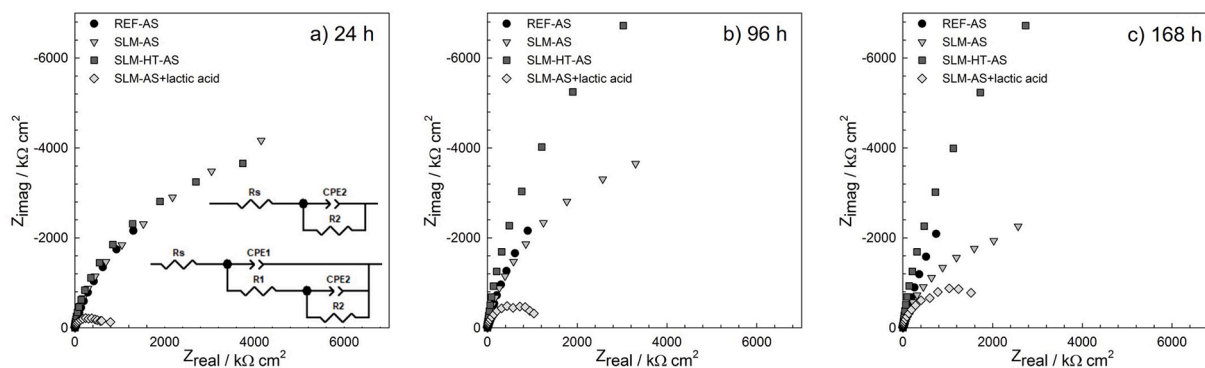


Fig. 3. Nyquist plots of the EIS measurements for the CoCr alloys in different environments (SLM – AS, SLM-HT – AS, REF – AS and SLM – AS + lactic acid) at a) 24 h, b) 96 h and c) 168 h of immersion. The inset in Fig. 3a represents equivalent circuits for fitting EIS data.

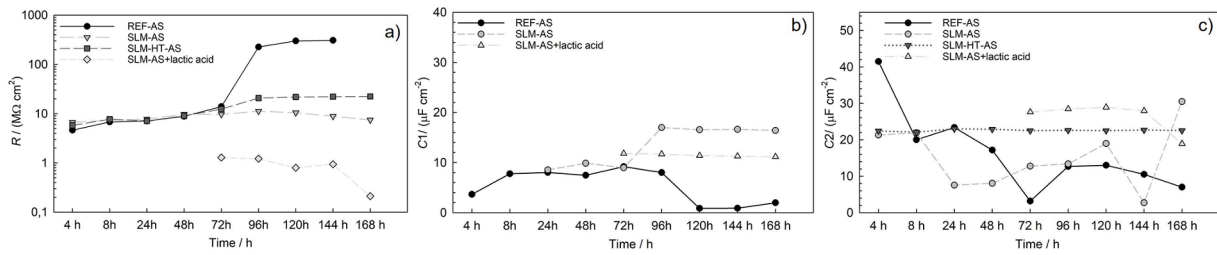


Fig. 4. Polarization resistance (a), capacitance C1 (b) and capacitance C2 (c) for the different CoCr specimens in artificial saliva and acidified artificial saliva at 37 °C during long immersion time.

passive layer either stopped growing or started to thin, as in the case of the SLM specimen in AS + lactic acid [49].

From equation:

$d = (\epsilon)(\epsilon_0)(A)/C_2$ , (3) where  $\epsilon$  is the dielectric constant of  $\text{Cr}_2\text{O}_3$ , which is equal to 12 [47,50],  $d$  is the thickness of the film,  $\epsilon_0$  is  $8.85 \cdot 10^{-14}$  F/cm and  $A$  is the surface area ( $\text{cm}^2$ ), it can be deduced that a decrease in the capacitance points to an increase in the thickness of the passive layer. This increase in thickness is bigger at early immersion

times. At the end of the immersion period (168 h), the calculated thicknesses of  $\text{Cr}_2\text{O}_3$  were 1.52 nm for the REF specimen, 0.35 nm for the SLM specimen, and 0.47 nm for the SLM-HT specimen, all in AS, and 0.56 nm for the SLM specimen in the AS + lactic acid.

### 3.3. Ion release tests

The results of the ion release tests, indicating the migration of

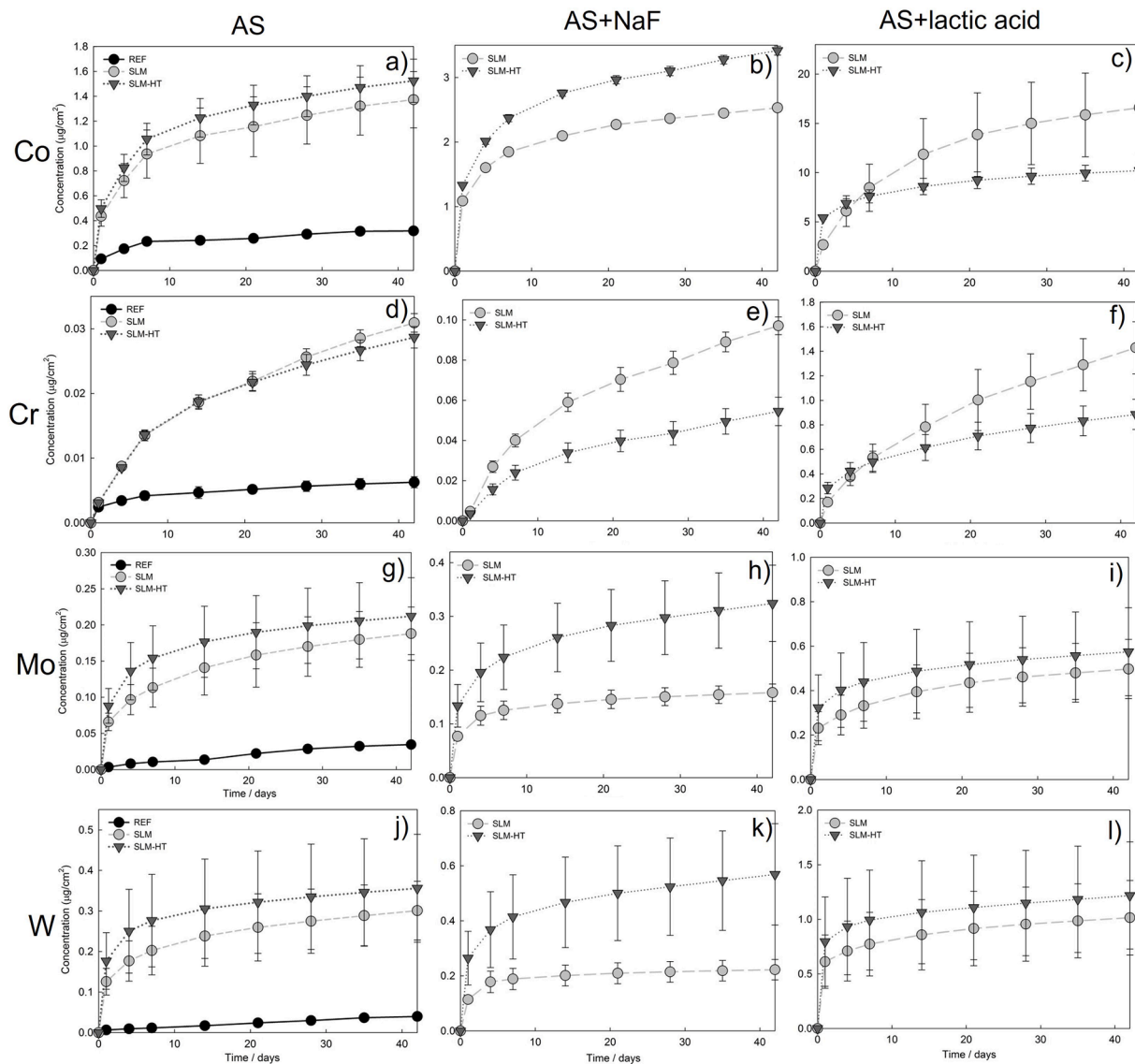


Fig. 5. Co, Cr, Mo and W released from SLM, SLM-HT and REF CoCr alloys over a 42-day period of exposure to artificial saliva, artificial saliva with 1450  $\mu\text{g/mL}$  of fluoride ions and acidified artificial saliva with lactic acid and a pH of 2.3.

alloying elements (Co, Cr, Mo and W) in the CoCr alloy investigated after exposure to AS, AS + NaF and AS + lactic acid are shown in Fig. 5. In these figures, the average cumulative concentrations of released metal ions and the associated standard errors, obtained from discrete measurements of three different samples, are plotted versus time.

Results showing the ion release of each individual element investigated following 42 days of exposure, as well as the total amount of ions released over this period, are presented in Table 3. The maximum allowed concentrations of all released ions from dental objects is defined in the standard ISO 22674: 2016, where it is prescribed not to exceed 200  $\mu\text{g}/\text{cm}^2$  after 7 days of exposure to saliva environments. In our case, the sum of the Co, Cr, Mo and W released, even after 42 days exposure (Table 3), i.e. the total mean ion release, considering the standard error – SE, was far below the maximum permissible concentrations. This indicates that investigate CoCr alloy (whether SLM printed or milled) are safe to use in dental applications. It can also be observed from Table 3 that, compared to AS, the total amount of ions released is higher in the AS + NaF, and even higher in the AS + lactic acid. In the AS environment, the total amount of metal ions released from the SLM and SLM-HT specimens is significantly higher than that from the REF sample ( $p(\text{SLM}/\text{REF})=0.027$  and  $p(\text{SLM-HT}/\text{REF})=0.014$ ). On the other hand, no significant difference was calculated between the ion release in the SLM and SLM-HT specimens in AS. In AS+NaF however, the total ion release was observed to be significantly higher in the SLM-HT specimen compared to the SLM one. In AS + lactic acid no significant differences were found between the materials compared (SLM vs. SLM-HT).

In AS at a neutral pH the mean release of Co ions (Fig. 5a) after 42 days of exposure is higher in the SLM and SLM-HT printed specimens (1.37 and 1.52  $\mu\text{g}/\text{mL}$ , respectively) than in the reference specimen (0.32  $\mu\text{g}/\text{mL}$ ). Statistical analysis showed this difference to be statistically significant, although there was no significant difference between the SLM and SLM-HT specimens. The release of Co ions is higher in AS + NaF than in AS, (see Fig. 5b), and significantly lower in the basic SLM printed specimens (2.53  $\mu\text{g}/\text{mL}$ ) compared to those that had been heat-treated (SLM-HT, 3.42  $\mu\text{g}/\text{mL}$ ). In the case of the samples exposed to AS + lactic acid, however, the trend is reversed – Co ions are released in higher concentration, with 16.6  $\mu\text{g}/\text{mL}$  released from the SLM samples and 10.2  $\mu\text{g}/\text{mL}$  from the SLM-HT samples (Fig. 5c). No significant difference was, however, found between the samples compared in this environment.

As can be seen in Fig. 5d-f, the amount of Cr ions released into the three different solutions is smaller in comparison to the migration of Co ions.

The SLM and SLM-HT samples released a similar amount of Cr ions into AS (0.03  $\mu\text{g}/\text{mL}$ ), with no significant difference found between them, while the REF sample released 3 times fewer Cr ions (0.01  $\mu\text{g}/\text{mL}$ ; Fig. 5d), a difference which was shown to be statistically significant

**Table 3**  
Mean ion release concentrations  $\pm$  SE (standard error) after 42 days of exposure (all results are given in  $\mu\text{g}/\text{cm}^2$ )\*.

	SLM AS	SLM-HT AS	REF AS	SLM AS+NaF	SLM-HT AS + NaF	SLM AS + lactic acid	SLM-HT AS + lactic acid
Co	1.37 $\pm 0.32$	1.52 $\pm 0.25$	0.32 $\pm 0.02$	2.53 $\pm 0.04$	3.42 $\pm 0.10$	16.6 $\pm 6.23$	10.2 $\pm 4.42$
Cr	0.03 $\pm 0.00$	0.03 $\pm 0.00$	0.01 $\pm 0.00$	0.10 $\pm 0.01$	0.05 $\pm 0.01$	1.42 $\pm 0.30$	0.86 $\pm 0.25$
Mo	0.19 $\pm 0.05$	0.21 $\pm 0.08$	0.03 $\pm 0.00$	0.16 $\pm 0.02$	0.32 $\pm 0.10$	0.50 $\pm 0.19$	0.57 $\pm 0.16$
W	0.30 $\pm 0.10$	0.36 $\pm 0.19$	0.04 $\pm 0.00$	0.22 $\pm 0.05$	0.57 $\pm 0.26$	1.01 $\pm 0.48$	1.21 $\pm 0.69$
Total	1.89 $\pm 0.48$	2.12 $\pm 0.51$	0.40 $\pm 0.00$	3.01 $\pm 0.12$	4.37 $\pm 0.47$	19.5 $\pm 7.20$	12.7 $\pm 5.53$

\* The ion release concentrations reported are the average and standard error obtained from discrete measurements of three different samples.

( $p < 0.001$ ). A higher amount of Cr ions are released into the AS + NaF, with the SLM-HT specimen releasing 50% fewer ions over the 42-day exposure period compared to the SLM specimen (0.05 and 0.10  $\mu\text{g}/\text{mL}$  respectively, Fig. 5e). No statistical difference was measured between the Cr ions release in these two specimens after the first day of exposure, but after that day a significant difference between the amount of Cr ions released from the two types of specimens was observed. In AS + lactic acid the amount of Cr ions released is higher compared to AS only or AS + NaF – with 1.42  $\mu\text{g}/\text{mL}$  released from SLM and 0.86  $\mu\text{g}/\text{mL}$  from SLM-HT (Fig. 5f). However, no significant difference is present between the results of Cr ion release from SLM and SLM-HT specimens in AS + lactic acid.

In the case of Mo ion release, it can again be observed that AS was the mildest corrosion media, with the lowest amount of Mo released in that environment (Fig. 5g) compared to the AS + NaF (Fig. 5h) and the AS + lactic acid (Fig. 5i). In AS the reference sample released a lower amount of Mo ions (0.04  $\mu\text{g}/\text{mL}$ ) than the SLM printed alloys (SLM = 0.19  $\mu\text{g}/\text{mL}$  and SLM-HT = 0.21  $\mu\text{g}/\text{mL}$ ). The interesting observation here is the behaviour of the SLM and SLM-HT samples, whereby the SLM-HT samples released a higher amount of Mo ions in all of the corrosive environments. It should, however, be pointed out that the statistical analysis showed no significant difference between the release of Mo ions in SLM and SLM-HT in any of the environments tested. In AS a significant difference was found between the amount of Mo ions released in the SLM-HT and REF specimens, but this was not consistent across all sampling days.

With respect to the release of W ions over 42 days of exposure at 37 °C, very similar trends are observed as to with Mo. In all three environments the highest amounts of W ions are released in the SLM-HT samples, and the lowest amount in the reference samples, which was only measured in AS (Fig. 5j-l).

Comparing the results given in Table 3 (total ion release after 42 days) and the graphs in Fig. 5j-l, relatively less W is released in AS than in AS + lactic acid, meaning that phases rich in W might preferentially dissolve in acidic artificial saliva environment. Statistical analysis, however, did not confirm a significant difference between the amount of W released from the specimens exposed to the three different environments.

#### 3.4. Surface roughness measurement on specimens for the ion migration test

The effect of surface roughness was studied in order to understand the different surface properties of the SLM printed and reference specimens. In this study the ion migration tests were carried out on specimens with the surface in the “as received condition”, which was sandblasted with 110  $\mu\text{m}$  particles of aluminium oxide, as they are prepared before tissue implantation and according to standard ISO 10271: 2020 - Dentistry — Corrosion test methods for metallic materials.

The starting surface condition of the SLM and REF specimens differs significantly. After sandblasting, both surfaces change. Images of the respective surfaces observed with a confocal microscope are given in Figs. 6a and b, with the alumina-sandblasted surfaces presented in Figs. 6c and d, respectively.

The surface roughness results of the as-received specimens, as measured by confocal microscopy, are presented in Table 4. The surface parameters  $S_a$ ,  $S_z$  and  $S_{dr}$  were determined on the SLM and REF specimens both before and after sand blasting.  $S_a$  is an extension of  $R_a$  – the mean arithmetical height of a line that expresses, as an absolute value, the difference in height of each point compared to the arithmetic mean of the surface. The maximum height ( $S_z$ ) is defined as the sum of the largest peak and the largest pit over the surface examined. The last parameter,  $S_{dr}$  (ratio of the interfacial area developed), is the percentage of the calculated area's additional surface area attributed to the texture as opposed to the planar area calculated [24,51,52].

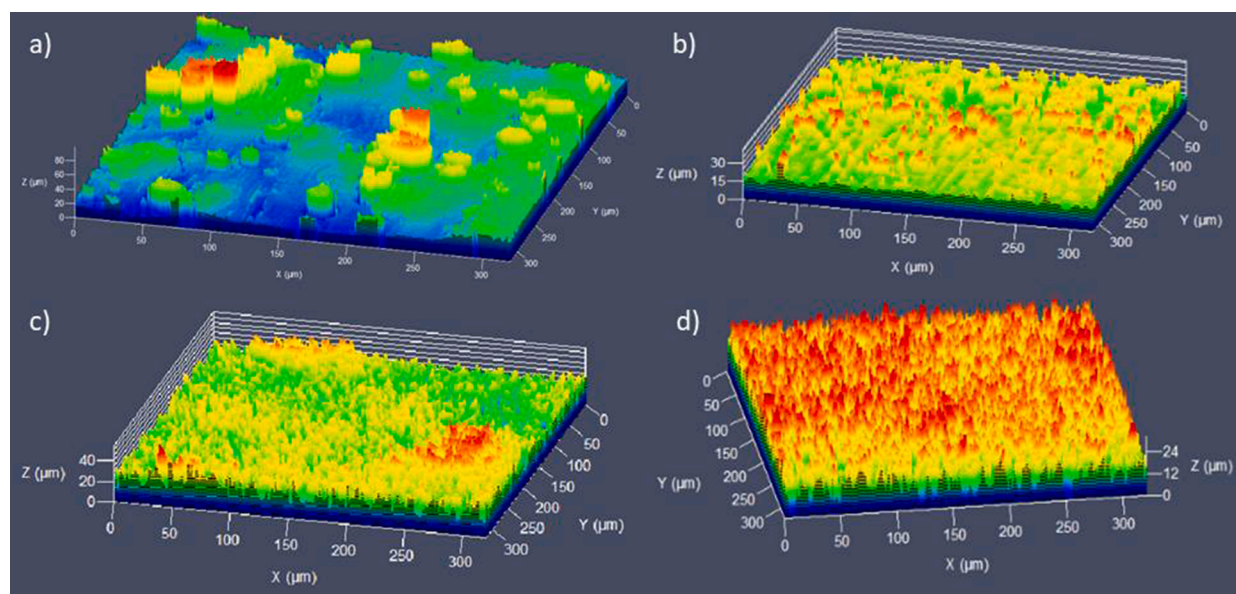


Fig. 6. Surfaces of the a) SLM, b) REF, c) alumina-blasted SLM and d) alumina-blasted REF examined by confocal microscopy.

Table 4

Results of surface analysis;  $S_a$  and  $S_{dr}$ \*.

	SLM (as built)	REF (milled)	SLM (alumina blasted)	REF (alumina blasted)
$S_a$ [ $\mu\text{m}$ ]	$15.6 \pm 3.1$	$2.4 \pm 0.2$	$6.7 \pm 0.5$	$6.5 \pm 0.8$
$S_z$ [ $\mu\text{m}$ ]	$74.1 \pm 9.0$	$4.0 \pm 1.7$	$35.7 \pm 1.5$	$31.1 \pm 1.8$
$S_{dr}$ [%]	$2099 \pm 206$	$12.5 \pm 0.4$	$1444 \pm 57.6$	$1277 \pm 13.9$
$R_a$ [ $\mu\text{m}$ ]	$9.4 \pm 1.3$	$0.5 \pm 0.1$	$2.3 \pm 0.5$	$1.2 \pm 0.1$
$R_z$ [ $\mu\text{m}$ ]	$50.9 \pm 4.1$	$4.0 \pm 0.8$	$13.7 \pm 2.1$	$8.9 \pm 0.9$

\* The reported values of  $S_a$ ,  $S_z$ ,  $S_{dr}$ ,  $R_a$  and  $R_z$  are the average and standard deviations obtained from discrete measurements of each sample at three different locations.

The actual exposed surfaces ( $S_{dr}$ ) differ from those that were calculated for ion migration test needs. The number of ions eluted from the exposed surface depends on the area exposed, which can be calculated from the outer dimensions of the object exposed. It can be seen from the results of the surface examination that, regardless of the initial surface condition, sandblasting with  $110 \mu\text{m}$  particles of aluminium oxide, provides a very unique surface morphology, with not only the  $S_{dr}$  being similar, but also the parameters  $S_a$  and  $S_z$ . The  $S_{dr}$  parameters for the alumina-sandblasted area are, however, very high: 1500% means the area is 15 times larger than the nominal dimensions of the object tested. Since all the specimens intended for the ion migration test were prepared in the same manner, the effect of the surface roughness was verified and proven to have a similar effect on the results of all the ion migration tests.

#### 4. Discussion

The main aim of the present in vitro study was to compare the resistance of corrosion over time, its progress over time, and the subsequent release of ions from chemically identical, but differently manufactured CoCr dental alloys. This infers that the corrosion resistance compared is not influenced by the chemistry of the alloys, but rather solely by the method of production. Through the temperature and cooling rate of the process the method of production thus dictates the development of a different microstructure and its interaction with the

environment throughout its service life.

The ion release concentrations measured from the materials investigated in different types of AS, representing the various oral environments possible (neutral, with excessive fluoride concentration, and with added lactic acid, as influenced by the inflammatory process), are herein interpreted by the results of the electrochemical tests and the microstructural features.

Potentiodynamic electrochemical measurements show that the passive current, indicating the quality of the passive layer, does not differ between the different specimens nor with a changing environment. The main reason for this is the similar chemical composition, especially with respect to the concentration of Cr, which plays the crucial role in the formation of the passive layer, and affects its thickness and composition. On the other hand, the open circuit potential ( $E_{OCP}$ ) measured during the conditioning period, the breakdown potential ( $E_b$ ), and the difference between  $E_b$  and  $E_{CORR}$  show that the best corrosion behaviour in AS can be attributed to the REF specimens, and the worst to SLM-HT. In AS + NaF, the best and the worst are SLM and SLM-HT, respectively. Overall, in all specimens tested the corrosion behaviour is better in AS + lactic acid than in the plain AS or the AS + NaF. In AS + lactic acid, however, the REF specimens show the lowest corrosion resistance, and SLM-HT the best. A similar, although not identical, behaviour, is also confirmed by the results of the polarization resistance, which was highest (indicating the best corrosion resistance, value  $R_p$ ) in the AS + lactic acid for the SLM specimen, followed by the REF and SLM-HT specimens. Because of the lower rate of potential increase from the cathodic to the anodic region, polarization resistance measured by the linear polarization technique is more accurate than results obtained by potentiodynamic polarization, where the potential increases 10 times faster. A specific observation for the potentiodynamic polarization is that the  $E_b$  potential is related to the environment to which the specimens are exposed (regardless of the specimen type). Passive current density, on the other hand, is neither related to the manufacturing process nor the environment.

From the results of long-term EIS measurements, and their additional analysis, it could be confirmed that the  $R$  values increase, while C2 remains constant, meaning that in the REF and SLM-HT specimens exposed to AS the passive layer improves over the measurement period. In the AS + lactic acid, on the other hand, despite the layer being thicker than that on both SLM specimens in AS, the value of C2 is constant, and  $R$  decreases, indicating that the passive layer stopped growing or started

to lose its protective behaviour by becoming porous [49]. This coincides well with the increased ion release measured in artificial saliva with added lactic acid compared to in the plain one. In plain AS, the corrosion performance and concentrations of ions released was similar in the SLM and SLM-HT specimens, with the difference being statistically insignificant. The lowest ion release was measured on the REF specimen in artificial saliva, and this difference was statistically significant. This was also confirmed by analysis of the long-term impedance measurements, namely calculation of the thickness of the passive layer, which in AS was highest for the REF specimen. This observation from our study is, however, in contradiction with results from the literature [3,53], where SLM specimens show better corrosion resistance and lower ion release than specimens produced by conventional methods. The far lower ion release from the REF sample could be a result of the more homogenous microstructure, which in turn provides the formation of a more homogeneous oxide development compared to the SLM samples. Furthermore, the metallographic analysis indicates that a strong formation of additional phases occurred in the SLM samples, which also depleted alloying elements from the material matrix. In turn, the chemical and phase heterogeneity could induce the development of other, less stable, passive layers that can later also cause the material to open on a local scale and increase corrosion progression in the underlying material, leading to a higher release of ions. Another possible explanation is the significantly higher presence of defects and interfaces in the SLM samples, which in turn can produce weak points for increased corrosive attack. This, in turn, could also explain why the corrosion behaviour is slightly improved when the SLM samples undergo heat treatment, which enables homogenization and recovery of the microstructure. amongst all the ions measured, the highest ion release was measured for Co. The concentrations of Cr, W and Mo ions released are not related to their concentrations in the alloy. Namely, the percentage of W and Mo released in the solution is almost in all tested cases higher than their respective amounts in the alloy (calculations given in Table 1). The opposite was observed for Cr which amount in the alloy is 27%, while the amount of Cr ions in the different saliva environments varies between 0.01  $\mu\text{g}/\text{cm}^2$  and 1.3  $\mu\text{g}/\text{cm}^2$ , which is between 2.3% and 7.3% of the total ions released for a particular system tested. This is due to the formation of a passive film, the main constituent of which is Cr, at least in freely corroding systems [54].

In the case of Co, a significantly higher amount of ions were released from SLM-HT into the AS + NaF compared to the SLM and REF (only in AS) specimens, whereas the amount of Co ions released in the acidic AS was significantly higher for SLM ( $p < 0.05$ ). The release of Cr ions was highest in the SLM specimens in all environments, which can be related to the fact that the matrix is in the least relaxed state, as a result of the rapid cooling during the SLM process. This, in turn, allows the formation of instable solid solutions with high chemical differences on a local scale. From this result it can be assumed that, based on passivation, and the formation of primarily Cr-oxide, but also Co-oxide, on the surface, corrosion resistance is improved by heat treatment. This assumption is confirmed by calculating the passive layer thickness from long-term EIS measurements. Additionally, the heat treatment causes partitioning of the alloying elements through the formation of additional phases, which causes the formation of more noble patches of the material present on the surface [27,33,35]. This reduces the amount of matrix material exposed and with it reduces the release of Cr and Co through oxide degradation. In the case of the AS + lactic acid, however, the additional Co-rich phases could also be involved in the corrosive degradation of the material, thus leading to the faster release of Co overall. In all the environments tested, the highest mean concentrations of W and Mo ions released were measured for the heat-treated SLM specimens, but no significant differences were confirmed by statistical analysis. During ageing at elevated temperatures, the  $\sigma$ -phase, rich in these two alloying, participates elements in grain boundaries. It has been observed by researchers [55] that an increase in the  $\sigma$ -phase has no influence on the release of Co ions, but increasing the amount in the alloy increases the

concentration of Cr and Mo released. In our study, the Cr ion release measurements did not confirm trend referred before, but this was observed for the release of Mo [55,56]. The cellular or columnar microstructure of the SLM specimens is enriched with Cr and Mo on the cell boundaries [57]. Since this unique microstructure completely disappears when the SLM specimens are heat-treated, but the corrosion properties are comparable to SLM as fabricated microstructure, this cannot be the main reason for the better corrosion performance of the milled specimens of this alloy.

In the case of our study, the total amount of ions released increased 6 (for SLM-HT) to 10 (for SLM specimens) times when changing the environment from AS to an AS + lactic acid. This is in agreement with other research [15,23,24,58]. In our study the results of electrochemical tests on specimens exposed to AS + lactic acid show the opposite, which could lead to a misleading conclusion. Results of the potentiodynamic measurements and the ion release tests can be successfully proved by the results of the long-term EIS experiment. The long-term impedance measurement in this study was recognized as a good tool for monitoring the passivation/ corrosion development of an environment/ metal system. By comparing the results of the EIS and ion migration tests it was observed that these two types of investigation complement one another, and the overall information gained is therefore more complete.

The ion release concentrations measured in our study were higher than those found in the literature [15,59]. The surface characteristics were therefore investigated as a possible reason for this discrepancy. Examination of the surfaces of the exposed specimens revealed the differences between the as-build (SLM and SLM-HT) and manufactured (REF) specimens. Since it was expected that the heat treatment would influence the geometry of the samples, because of the stress relief function, but not the micro appearance of the surface, it was assumed that the SLM specimens (both with and without heat treatment) would not differ significantly in this parameter. Sandblasting using 110  $\mu\text{m}$  particles of aluminium oxide-alumina ( $\text{Al}_2\text{O}_3$ ) decreased the  $S_{\text{dr}}$  of the original SLM surface, but increased the  $S_{\text{dr}}$  on the specimens milled from prefabricated blocks. By comparing the alumina-sandblasted surfaces of the SLM and REF specimens, it could be seen that the SLM sandblasted surface was 14.4 times larger than the calculated surface, while the developed surface of the REF samples was 12.8 times larger. If we take this parameter into consideration and normalize the ion release concentrations, the concentrations in the REF samples are still approximately 3 times lower than those of the SLM or SLM-HT specimens, which means that, despite fabrication by casting, the microstructure of the REF specimen is less sensitive to corrosion, as was described earlier in this manuscript. The  $S_{\text{dr}}$  parameter measured on the alumina-sandblasted specimens could also explain the higher concentrations of released ions measured compared to those reported in the literature. In one study on polished SLM specimens, for example, the concentration of Co ions released into artificial acidic saliva after 7 days of exposure was measured to be 0.685  $\mu\text{g}/\text{cm}^2$  [15], whereas the concentration measured in a similar solution after the same period of time in our case was far higher, at 7.535  $\mu\text{g}/\text{cm}^2$ . When we normalized this result, by considering the  $S_{\text{dr}}$  parameter, a comparable concentration of 0.523  $\mu\text{g}/\text{cm}^2$  was obtained. Here, a significant effect of the surface condition on the release of ions is clearly demonstrated.

Sandblasting with aluminium oxide particles, a necessary surface treatment that is routinely used in dentistry [60], significantly increases the real surface on a micro level, by up to 15 times more than the nominal level. The differences between the nominal surfaces of the differently manufactured specimens were reduced by sandblasting. It can be seen from the results of the ion migration measurements, however, that the lowest concentrations were measured in the REF specimens. This might have also contributed to the lower real exposed area in this type of specimen. In order to prove this, however, additional study should be carried out on specimens of the same type investigating the effect of differently machined surfaces (as well as alumina-blasted also as-fabricated and polished surfaces, for example).

## 5. Conclusion

From the results of the present in vitro study the following conclusions can be drawn:

The CoCr alloy manufactured by SLM releases higher ion concentrations in AS than those manufactured by milling, where the original condition is cast block. The difference between the non-heat-treated and the heat-treated SLM specimens is not significant in this environment. From a clinical perspective this means that heat treatment of the SLM printed restorations has no impact on the corrosion properties of this particular CoCr alloy.

Long-term electrochemical impedance spectroscopy measurements revealed the formation of a passive layer over time, whereby in AS the most stable and thickest passive layer is formed on REF specimens, which released the lowest quantity of ions. In AS with lactic acid, where the highest total release of metal ions was measured, a less protective passive layer is formed, which undergoes thinning over time. In clinical conditions this means that the CoCr alloys will probably exhibit higher corrosivity in patients with a chronic acidic oral environment.

The concentration of eluted elements is somehow proportional to its concentration in the alloy, with the exception of Cr, the release of which into AS and AS with NaF is the lowest amongst all the elements monitored, indicating its role in the formation of a stable and high-quality Cr-oxide layer in these environments. The release of Cr ions in AS with lactic acid is, however, higher, due to deterioration of the passive layer in this media.

The real interfacial area, defined as  $S_{dr}$ , plays a crucial role in the release of metal ions – the total amount of metal ions released is proportional to the actual area of the surface exposed to the environment to the environment.

Additional analysis of the structure of the passive film is envisioned, but the implementation of such analysis is beyond the scope of this paper.

## CRedit authorship contribution statement

**Mirjam Bajt Leban:** Conceptualization, Methodology, Data curation, Writing – original draft. **Matej Kurnik:** Formal analysis, Writing – review & editing. **Igor Kopač:** Formal analysis, Writing – review & editing. **Matic Jovičević Klug:** Writing – review & editing. **Bojan Podgornik:** Writing – review & editing. **Tadeja Kosec:** Writing – review & editing, Formal analysis, Supervision, Validation, Funding acquisition.

## Declaration of Competing Interest

The authors declare that they have no known competing financial interests or personal relationships that could have appeared to influence the work reported in this paper.

The authors declare the following financial interests/personal relationships which may be considered as potential competing interests.

## Data availability

Data will be made available on request.

## Acknowledgments

This work is based on the research project Implementation of additive technologies in prosthodontics supported by the Slovenian Research Agency (grant No. L2-1831).

## Supplementary materials

Supplementary material associated with this article can be found, in

the online version, at [doi:10.1016/j.electacta.2023.142066](https://doi.org/10.1016/j.electacta.2023.142066).

## References

- [1] J.L. Ferencz, N.R.F.A. Silva, J.M. Navarro (Eds.), *High-strength Ceramics: Interdisciplinary Perspectives*, Quintessence Publishing Co., Inc, Hanover Park, IL, 2014. ISBN: 978-0-86715-639-3.
- [2] R. van Noort, The future of dental devices is digital, *Dent. Mater.* 28 (2012) 3–12, <https://doi.org/10.1016/j.dental.2011.10.014>.
- [3] X. Xin, J. Chen, N. Xiang, B. Wei, Surface properties and corrosion behavior of Co–Cr alloy fabricated with selective laser melting technique, *Cell Biochem. Biophys.* 67 (2013) 983–990, <https://doi.org/10.1007/s12013-013-9593-9>.
- [4] N. Dolgov, T. Dikova, D. Dzhendov, D. Pavlova, M. Simov, Mechanical properties of dental Co–Cr alloys fabricated via casting and selective laser melting, *Int. J. Mater. Sci. Non-Equilib. Phase Transform.* (2016) 3–7. ISSN 1310-3946. <https://innovaeng.eu/proceedings/2016/09.MECHANICAL%20PROPERTIES%20OF%20DENTAL%20CoCr%20ALLOYS%20FABRICATED%20VIA%20CASTING%20AND%20SELECTIVE%20LASER%20MELTING.pdf>.
- [5] H. Kim, S.-H. Jang, Y. Kim, J. Son, B. Min, K.-H. Kim, T.-Y. Kwon, Microstructures and mechanical properties of Co–Cr dental alloys fabricated by three CAD/CAM-based processing techniques, *Materials (Basel)* 9 (2016) 596, <https://doi.org/10.3390/ma9070596>.
- [6] S. Liu, Y.C. Shin, Additive manufacturing of Ti6Al4V alloy: a review, *Mater. Des.* 164 (2019), 107552, <https://doi.org/10.1016/j.matdes.2018.107552>.
- [7] Q. Sui, P. Li, K. Wang, X. Yin, L. Liu, Y. Zhang, Q. Zhang, S. Wang, L. Wang, Effect of build orientation on the corrosion behavior and mechanical properties of selective laser melted Ti-6Al-4V, *Metals* 9 (2019) 976, <https://doi.org/10.3390/met9090976>.
- [8] J. Alcisto, A. Enriquez, H. Garcia, S. Hinkson, T. Steelman, E. Silverman, P. Valdivino, H. Gigerenzer, J. Foyos, J. Ogren, J. Dorey, K. Karg, T. McDonald, O. S. Es-Said, Tensile properties and microstructures of laser-formed Ti-6Al-4V, *J. Mater. Eng. Perform.* 20 (2011) 203–212, <https://doi.org/10.1007/s11665-010-9670-9>.
- [9] D.A. Hollander, M. von Walter, T. Wirtz, R. Sellei, B. Schmidt-Rohlfing, O. Paar, H.-J. Erli, Structural, mechanical and in vitro characterization of individually structured Ti-6Al-4V produced by direct laser forming, *Biomaterials* 27 (2006) 955–963, <https://doi.org/10.1016/j.biomaterials.2005.07.041>.
- [10] M. Rüger, T.J. Gensior, C. Herren, M. von Walter, C. Ocklenburg, R. Marx, H.-J. Erli, The removal of Al<sub>2</sub>O<sub>3</sub> particles from grit-blasted titanium implant surfaces: effects on biocompatibility, osseointegration and interface strength in vivo, *Acta Biomater.* 6 (2010) 2852–2861, <https://doi.org/10.1016/j.actbio.2010.01.009>.
- [11] M. Akbar, J.M. Brewer, M.H. Grant, Effect of chromium and cobalt ions on primary human lymphocytes in vitro, *J. Immunotoxicol.* 8 (2011) 140–149, <https://doi.org/10.3109/1547691X.2011.553845>.
- [12] G.O. Alrabeah, P. Brett, J.C. Knowles, H. Petridis, The effect of metal ions released from different dental implant-abutment couples on osteoblast function and secretion of bone resorbing mediators, *J. Dent.* 66 (2017) 91–101, <https://doi.org/10.1016/j.jdent.2017.08.002>.
- [13] J.C. Wataha, Alloys for prosthodontic restorations, *J. Prosthet. Dent.* 87 (2002) 351–363, <https://doi.org/10.1067/mp.2002.123817>.
- [14] J. Li, H. Ren, C. Liu, S. Shang, The effect of specific energy density on microstructure and corrosion resistance of CoCrMo alloy fabricated by laser metal deposition, *Materials (Basel)* 12 (2019) 1321, <https://doi.org/10.3390/ma12081321>.
- [15] T. Puskar, D. Jevremovic, R. Williams, D. Eggbeer, D. Vukelic, I. Budak, A comparative analysis of the corrosive effect of artificial saliva of variable pH on DMLS and cast Co–Cr–Mo dental alloy, *Materials (Basel)* 7 (2014) 6486–6501, <https://doi.org/10.3390/ma7096486>.
- [16] M. Seyedi, F. Zanotto, C. Monticelli, A. Balbo, E. Liverani, A. Fortunato, Microstructural characterization and corrosion behaviour of SLM CoCrMo alloy in simulated body fluid, *Metall. Ital.* 110 (2018) 45–50.
- [17] A. Takaichi, T. Nakamoto Suyalatu, N. Joko, N. Nomura, Y. Tsutsumi, S. Migita, H. Doi, S. Kurosu, A. Chiba, N. Wakabayashi, Y. Igarashi, T. Hanawa, Microstructures and mechanical properties of Co–29Cr–6Mo alloy fabricated by selective laser melting process for dental applications, *J. Mech. Behav. Biomed. Mater.* 21 (2013) 67–76, <https://doi.org/10.1016/j.jmbbm.2013.01.021>.
- [18] K. Monroy, J. Delgado, J. Ciurana, Study of the pore formation on CoCrMo alloys by selective laser melting manufacturing process, *Procedia Eng.* 63 (2013) 361–369, <https://doi.org/10.1016/j.proeng.2013.08.227>.
- [19] G. Cui, H. Liu, S. Li, G. Gao, M. Hassani, Z. Kou, Effect of Ni, W and Mo on the microstructure, phases and high-temperature sliding wear performance of CoCr matrix alloys, *Sci. Technol. Adv. Mater.* 21 (2020) 229–241, <https://doi.org/10.1080/14686996.2020.1752113>.
- [20] A. Karaali, K. Mirouh, S. Hamamda, P. Guiraldenq, Microstructural study of tungsten influence on Co–Cr alloys, *Mater. Sci. Eng. A Struct. Mater.* 390 (2005) 255–259, <https://doi.org/10.1016/j.msea.2004.08.001>.
- [21] H. Matusiewicz, Potential release of in vivo trace metals from metallic medical implants in the human body: from ions to nanoparticles—a systematic analytical review, *Acta Biomater.* 10 (2014) 2379–2403, <https://doi.org/10.1016/j.actbio.2014.02.027>.
- [22] G. Sander, J. Tan, P. Balan, O. Gharbi, D.R. Feenstra, L. Singer, S. Thomas, R.G. Kelly, J.R. Scully, N. Birbilis, Corrosion of Additively Manufactured Alloys: A Review, *CORROSION*. 74 (2018) 1318–1350. [10.5006/2926](https://doi.org/10.5006/2926).
- [23] R. Padrós, L. Giner-Tarrida, M. Herrero-Climent, M. Punset, F.J. Gil, Corrosion resistance and ion release of dental prosthesis of CoCr obtained by CAD-CAM

- milling, casting and laser sintering, *Metals (Basel)* 10 (2020) 827, <https://doi.org/10.3390/met10060827>.
- [24] M. Kassapidou, L. Hjalmarsson, C.B. Johansson, P. Hammarström Johansson, E. Morisbak, A. Wennerberg, V. Franke Stenport, Cobalt–chromium alloys fabricated with four different techniques: ion release, toxicity of released elements and surface roughness, *Dent. Mater.* 36 (2020) e352–e363, <https://doi.org/10.1016/j.dental.2020.08.012>.
- [25] S.H. Tuna, E. Karaca, İ. Aslan, G. Pekkan, N.Ö. Pekmez, Evaluation of corrosion resistance of Co-Cr alloys fabricated with different metal laser sintering systems, *J. Adv. Prosthodont.* 12 (2020) 114, <https://doi.org/10.4047/jap.2020.12.3.114>.
- [26] T. Aldhohrah, J. Yang, J. Guo, H. Zhang, Y. Wang, Ion release and biocompatibility of Co-Cr alloy fabricated by selective laser melting from recycled Co-Cr powder: an in vitro study, *J. Prosthet. Dent.* (2021), <https://doi.org/10.1016/j.prosdent.2021.09.003>, S0022391321004911.
- [27] K.M. Mantrala, M. Das, V.K. Balla, Ch.S. Rao, V.V.S. Kesava Rao, Additive manufacturing of Co-Cr-Mo alloy: influence of heat treatment on microstructure, tribological, and electrochemical properties, *Front. Mech. Eng.* (2015) 1, <https://doi.org/10.3389/fmech.2015.00002>.
- [28] A. Charimi, R. Falkenberg, L. Ávila, G. Mohr, K. Sommer, A. Ulbricht, M. Sprengel, R. Saliwan Neumann, B. Skrotzki, A. Evans, Mechanical anisotropy of additively manufactured stainless steel 316L: an experimental and numerical study, *Mater. Sci. Eng. A Struct. Mater.* 799 (2021), 140154, <https://doi.org/10.1016/j.msea.2020.140154>.
- [29] Y. Bedolla-Gil, A. Juárez-Hernández, A.J. Pérez-Unzueta, E. García-Sánchez, R. D. Mercado-Solís, M.A.L. Hernandez-Rodriguez, Influence of heat treatments on mechanical properties of a biocompatibility alloy ASTM F75, *Rev. Mex. Fis.* 55 (2009) 1–5.
- [30] W.-F. Lee, J.-C. Wang, C.-Y. Hsu, P.-W. Peng, Microstructure, mechanical properties, and retentive forces of cobalt-chromium removable partial denture frameworks fabricated by selective laser melting followed by heat treatment, *J. Prosthet. Dent.* (2020), <https://doi.org/10.1016/j.prosdent.2020.06.038>, S0022391320305667.
- [31] Y. Zhou, N. Li, J. Yan, Q. Zeng, Comparative analysis of the microstructures and mechanical properties of Co-Cr dental alloys fabricated by different methods, *J. Prosthet. Dent.* 120 (2018) 617–623, <https://doi.org/10.1016/j.prosdent.2017.11.015>.
- [32] X. Yan, H. Lin, Y. Wu, W. Bai, Effect of two heat treatments on mechanical properties of selective-laser-melted Co-Cr metal-ceramic alloys for application in thin removable partial dentures, *J. Prosthet. Dent.* 119 (2018) 1028.e1–1028.e6, <https://doi.org/10.1016/j.prosdent.2018.04.002>.
- [33] K. Dimitriadis, A.G. Lekatou, A.K. Sfikas, M. Roumpi, S. Tsouli, A. Galiatsatos, S. Agathopoulos, Influence of heat-treatment cycles on the microstructure, mechanical properties, and corrosion resistance of Co-Cr dental alloys fabricated by selective laser melting, *J. Mater. Eng. Perform.* 30 (2021) 5252–5265, <https://doi.org/10.1007/s11665-021-05738-9>.
- [34] Y. Zhou, Q. Sun, X. Dong, N. Li, Z.J. Shen, Y. Zhong, M. Eriksson, J. Yan, S. Xu, C. Xin, Microstructure evolution and mechanical properties improvement of selective laser melted Co-Cr biomedical alloys during subsequent heat treatments, *J. Alloys Compd.* 840 (2020), 155664, <https://doi.org/10.1016/j.jallcom.2020.155664>.
- [35] D. Rylska, B. Januszewicz, G. Sokolowski, J. Sokolowski, Corrosion resistance of Cr–Co alloys subjected to porcelain firing heat treatment—in vitro study, *Processes* 9 (2021) 636, <https://doi.org/10.3390/pr9040636>.
- [36] W. Wei, Y. Zhou, Q. Sun, N. Li, J. Yan, H. Li, W. Liu, C. Huang, Microstructures and mechanical properties of dental Co-Cr-Mo-W alloys fabricated by selective laser melting at different subsequent heat treatment temperatures, *Metall. Mater. Trans. A* 51 (2020) 3205–3214, <https://doi.org/10.1007/s11661-020-05719-y>.
- [37] Y. Kajima, A. Takaichi, N. Kittikundecha, T. Nakamoto, T. Kimura, N. Nomura, A. Kawasaki, T. Hanawa, H. Takahashi, N. Wakabayashi, Effect of heat-treatment temperature on microstructures and mechanical properties of Co–Cr–Mo alloys fabricated by selective laser melting, *Mater. Sci. Eng. A Struct. Mater.* 726 (2018) 21–31, <https://doi.org/10.1016/j.msea.2018.04.048>.
- [38] M. Roudnicka, J. Bigas, O. Molnarova, D. Palousek, D. Vojtech, Different response of cast and 3D-printed Co-Cr-Mo alloy to heat treatment: a thorough microstructure characterization, *Metals (Basel)* 11 (2021) 687, <https://doi.org/10.3390/met11050687>.
- [39] K. Kulcsár, J. Kónya, The influence of heat treatment on the mechanical properties of 3D-printed cobalt-chrome alloy used in dental laboratory practice, *Acta Mater. Transilv.* 1 (2018) 97–100, <https://doi.org/10.2478/amt-2018-0036>.
- [40] G.S. Duffó, E.Q. Castillo, Development of an artificial saliva solution for studying the corrosion behavior of dental alloys, *Corrosion* 60 (2004) 594–602, <https://doi.org/10.5006/1.3287764>.
- [41] M.R. Alkahari, T. Furumoto, T. Ueda, A. Hosokawa, Melt pool and single track formation in selective laser sintering/selective laser melting, *AMR.* 933 (2014) 196–201, [10.4028/www.scientific.net/AMR.933.196](https://doi.org/10.4028/www.scientific.net/AMR.933.196).
- [42] T. Kosce, M. Bajt Leban, M. Kurnik, I. Kopač, Comparison of the corrosion properties of CoCrMo dental alloys in artificial saliva, *Mater. Tehnol.* 55 (2021), <https://doi.org/10.17222/mit.2021.283>.
- [43] S. Mercieca, M. Caligari Conti, J. Buhagiar, J. Camilleri, Assessment of corrosion resistance of cast cobalt-nickel-chromium and dental alloys in acidic environments, *J. Appl. Biomater. Funct. Mater.* 16 (2018) 47–54, <https://doi.org/10.5301/jabfm.5000383>.
- [44] A.W.E. Hodgson, S. Kurz, S. Virtanen, V. Fervel, C.-O.A. Olsson, S. Mischler, Passive and transpassive behaviour of CoCrMo in simulated biological solutions, *Electrochim. Acta* 49 (2004) 2167–2178, <https://doi.org/10.1016/j.electacta.2003.12.043>.
- [45] A.I. Mun-oz, S. Mischler, Interactive effects of albumin and phosphate ions on the corrosion of CoCrMo implant alloy, *J. Electrochem. Soc.* 154 (2007) C562, <https://doi.org/10.1149/1.2764238>.
- [46] B. Seo, H.-K. Park, K.B. Park, H.-S. Kang, K. Park, Effect of hydrogen peroxide on Cr oxide formation of additive manufactured CoCr alloys during plasma electrolytic polishing, *Mater. Lett.* 294 (2021), 129736, <https://doi.org/10.1016/j.matlet.2021.129736>.
- [47] Y. Okazaki, Characterization of oxide film of implantable metals by electrochemical impedance spectroscopy, *Materials (Basel)* (2019) 12, <https://doi.org/10.3390/ma12213466>.
- [48] D. Kek-Merl, J. Lappalainen, H.L. Tuller, Electrical properties of nanocrystalline CeO<sub>2</sub> thin films deposited by in situ pulsed laser deposition, *J. Electrochem. Soc.* 153 (2006), <https://doi.org/10.1149/1.2165778>, J15.
- [49] I.C. Lavos-Valereto, S. Wolyneć, I. Ramires, A.C. Guastaldi, I. Costa, Electrochemical impedance spectroscopy characterization of passive film formed on implant Ti–6Al–7Nb alloy in Hank's solution, *J. Mater. Sci. Mater. Med.* 15 (2004) 55–59, <https://doi.org/10.1023/B:JMSM.0000010097.86245.74>.
- [50] B.G. Pound, Electrochemical behavior of cobalt-chromium alloys in a simulated physiological solution, *J. Biomed. Mater. Res.* 94 (2010) 93–102, <https://doi.org/10.1002/jbm.a.32684>.
- [51] A. Townsend, L. Pagani, P.J. Scott, L. Blunt, Introduction of a surface characterization parameter sdrprime for analysis of re-entrant features, *J. Nondestruct. Eval.* 38 (2019) 58, <https://doi.org/10.1007/s10921-019-0573-x>.
- [52] B. Al-Nawas, H. Götz, Three-dimensional topographic and metrologic evaluation of dental implants by confocal laser scanning microscopy, *Clin. Implant Dent. Relat. Res.* 5 (2003) 176–183, <https://doi.org/10.1111/j.1708-8208.2003.tb00200.x>.
- [53] H.M. Hamza, K.M. Deen, W. Haider, Microstructural examination and corrosion behavior of selective laser melted and conventionally manufactured Ti6Al4V for dental applications, *Mater. Sci. Eng. C* 113 (2020), 110980, <https://doi.org/10.1016/j.msec.2020.110980>.
- [54] I. Milošev, H.-H. Strehlow, The composition of the surface passive film formed on CoCrMo alloy in simulated physiological solution, *Electrochim. Acta* 48 (2003) 2767–2774, [https://doi.org/10.1016/S0013-4686\(03\)00396-7](https://doi.org/10.1016/S0013-4686(03)00396-7).
- [55] S. Kurosu, N. Nomura, K. Yamaguchi, S. Fujinuma, A. Chiba, Effects of 5th element addition to Co-29Cr-6Mo alloy containing impurity Ni on metal ion release, *J. Japan Inst. Metals* 69 (2005) 886–891, <https://doi.org/10.2320/jinstmet.69.886>.
- [56] J.S. Kasper, B.F. Decker, J.R. Belanger, The crystal structure of the sigma-phase in the Co-Cr system, *J. Appl. Phys.* 22 (1951) 361–362, <https://doi.org/10.1063/1.1699960>.
- [57] Y. Kajima, A. Takaichi, N. Kittikundecha, H.L. Htat, H.H.W. Cho, Y. Tsutsumi, T. Hanawa, N. Wakabayashi, T. Yoneyama, Reduction in anisotropic response of corrosion properties of selective laser melted Co–Cr–Mo alloys by post-heat treatment, *Dent. Mater.* 37 (2021) e98–e108, <https://doi.org/10.1016/j.dental.2020.10.020>.
- [58] M. Arregui, F. Latour, F.J. Gil, R.A. Pérez, L. Giner-Tarrida, L.M. Delgado, Ion release from dental implants, prosthetic abutments and crowns under physiological and acidic conditions, *Coatings* 11 (2021) 98, <https://doi.org/10.3390/coatings11010098>.
- [59] X.-Z. Xin, J. Chen, N. Xiang, Y. Gong, B. Wei, Surface characteristics and corrosion properties of selective laser melted Co–Cr dental alloy after porcelain firing, *Dent. Mater.* 30 (2014) 263–270, <https://doi.org/10.1016/j.dental.2013.11.013>.
- [60] B. Konieczny, A. Szczesio-Włodarczyk, J. Sokolowski, K. Bociąg, Challenges of Co–Cr alloy additive manufacturing methods in dentistry—the current state of knowledge (Systematic Review), *Materials (Basel)* 13 (2020) 3524, <https://doi.org/10.3390/ma13163524>.